Kinetic analysis of an efficient, molecular light-driven water oxidation system

Laia Francàs,[1,2*] Roc Matheu,[2,3] Ernest Pastor,[1,¶] Anna Reynal,[1,4] Serena Berardi,[2,ξ] Xavier Sala,[5] Antoni Llobet[2,5*] and James R. Durrant[1]

Addresses

1 Department of Chemistry, Imperial College London, South Kensington Campus, London, SW7 2AZ, United Kingdom.

2 Institute of Chemical Research of Catalonia (ICIQ), Avinguda Països Catalans 16, 43007 Tarragona, Spain.

3 Departament de Química Física i Inorgànica, Universitat Rovira i Virgili, Marcel·lí Domingo s/n, 43007 Tarragona, Spain.

4 Department of Science, Teesside University, Borough Road, Middlesbrough, TS1 3BA, United Kingdom.

5 Departament de Química, Universitat Autònoma de Barcelona, Cerdanyola del Vallès, 08193 Barcelona, Spain.

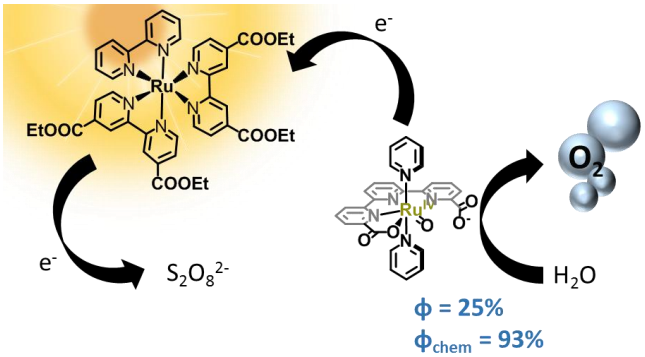

ABSTRACT: We report an efficient molecular light-driven system to oxidize water to oxygen and the kinetic analysis of the factors determining the efficiency of the system. The system comprises a highly active molecular catalyst ($[Ru^{IV}(tda)(py)_2(O)]$), $[Ru^{II}(bpy)(bpy\text{-}COOEt)_2]^{2+}$ (**RuP**) as sensitizer and $Na_2S_2O_8$ as sacrificial electron acceptor. This combination exhibits a high quantum yield (25%) and chemical yield (93%) for photo-driven oxygen evolution from water. The processes underlying this performance are identified using optical techniques including transient absorption spectroscopy and photoluminescence quenching. A high catalyst concentration is found to be required to optimize the efficiency of electron transfer between the oxidized sensitizer and the catalyst, which also has the effect of improving sensitizer stability. The main limitation of the quantum yield is the relatively low efficiency of $S_2O_8^{2-}$ as an electron scavenger to oxidize the photoexcited ruthenium sensitizer **RuP*** to 2 **RuP**$^+$, mainly due to competing back electron transfers to the **RuP** ground state. The overall rate of light-driven oxygen generation is determined primarily by the rate of photon absorption by the molecular sensitizer under the incident photon flux. As such the performance of this efficient light-driven system is limited not by the properties of the molecular water oxidation catalyst, which exhibits both good kinetics and stability, but rather by the light absorption and quantum efficiency properties of the sensitizer and electron scavenger. We conclude by discussing the implications of these results for further optimization of molecular light-driven systems for water oxidation.

KEYWORDS: Light-driven catalysis, water oxidation, quantum yield, kinetics, oxygen generation.

1. INTRODUCTION

Harnessing solar energy to drive the synthesis of hydrogen from water, and the reduction of CO_2 to other fuels such as methanol, offers a renewable, carbon zero (for H_2) or neutral (CO_2 reduced fuels) pathway to reduce our dependency on fossil fuels. This process is called artificial photosynthesis, because it mimics plant's use of solar energy, water and CO_2 to store energy in chemical bonds. As in natural photosynthesis, one of the key processes that need to take place is water oxidation, in which four electrons and four protons are extracted from two water mole-

cules, producing molecular oxygen. This process is both kinetically and energetically demanding. A key challenge in this field is thus the development of suitable water oxidation catalysts (WOCs) that drive water oxidation induced by light. In recent years, substantial progress has been reported on molecular water oxidation catalysts[1,2] although light-driven water oxidation activity has been demonstrated in only a small number of cases.[3,4,5,6,7,8,9,10,11] Furthermore analyses of the kinetic processes determining the efficiency of these photoactivated systems, have been very limited to date and in several cases the molecular catalyst has been reported to degrade to the corresponding metal oxide.[3,6b,7,8,9a].

Homogeneous photoactivated water oxidation systems typically consist of ternary systems including a light harvesting molecule, such as $[Ru(bpy)_3]^{2+}$ (bpy is 2,2'-bipyridine; see Chart 1 for a chemical structures), a sacrificial electron acceptor, such as persulfate and a water oxidation catalyst. Amongst all the reported molecular water oxidation catalysts, ruthenium complexes exhibit the highest performances when driven both chemically and electrochemically. However, such catalysts often exhibit rather poor efficiencies when used in light-driven systems, with quantum yields for oxygen generation per incident photon typically being ≤ 10 %.[3,4a] These modest efficiencies for light-driven systems have typically been assigned to limitations associated with the low turnover frequencies (TOF) of the molecular water oxidation catalyst, as well as the severe overpotentials required to drive the catalytic reaction. As such, efforts in this field have been recently focused on improving both the overpotential requirements and TOF's for molecular water oxidation catalysts. It is worth mentioning here that increasing the catalyst-dye interactions via a supramolecular approach can also significantly enhance quantum yields.[5]

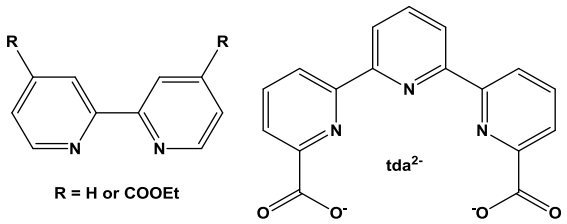

Chart 1. Key ligands used in this work

Recently, we have reported[2] a highly efficient Ru based water oxidation catalyst $[Ru^{IV}(tda)(py)_2(O)]$, (abbreviated from now on as **Ru^{IV}=O**; py is pyridine and tda^{2-} [2,2':6',2''-terpyridine]-6,6''-dicarboxylato; see Chart 1), that is generated in neutral or basic pH from its precursor $[Ru^{IV}(tda\text{-}\kappa\text{-}N^3O^2)(py)_2]$, **$Ru^{IV}$-tda**. The **$Ru^{IV}$=O** complex oxidizes water to dioxygen elecrocatalytically at pH = 7 with a maximum turnover frequency of 8,000 s^{-1} and is therefore an ideal candidate for use in light-driven catalysis. Herein, we have employed this catalyst in a ternary photoactivated system, using a Ru-bpy derivative as a sensitizer and persulfate as a sacrificial electron acceptor. This yields a remarkably efficient homogeneous light-driven water oxidation system. We have used electrochemical, steady state and transient spectroscopic techniques to study the key steps occurring in this three-component system and to obtain a detailed kinetic analysis of the different reactions involved, and the efficiencies of the key individual steps. Our study provides insight to loss pathways in light-driven molecular water oxidation systems and highlights potential routes of improvement.

2. RESULTS

2.1 Dark redox processes for the **Ru-tda** molecular catalyst.

We first consider the dark redox chemistry of the molecular water oxidation catalyst employed in this study. Recently we have reported a family of Ru complexes containing the pentadentate ligand tda^{2-} that coordinates the metal center in the equatorial plane so that the remaining two axial coordination positons can be occupied by monodentate ligands such as pyridine.[2] At ruthenium oxidation state II the tda^{2-} ligand binds in a tetradentate manner, $[Ru^{II}(tda\text{-}\kappa\text{-}N^3O)(py)_2]$, labelled as **$Ru^{II}$-tda** (Scheme 1) but upon two successive one-electron oxidation the latter yields the seven coordinate complex $[Ru^{IV}(tda\text{-}\kappa\text{-}N^3O^2)(py)_2]$, **$Ru^{IV}$-tda**, where now the tda^{2-} ligand acts in a pentadentate fashion as shown in the upper part of Scheme 1. As has been previously reported, pure samples of these complexes can be obtained either chemically or electrochemically by bulk electrolysis and have been individually characterized. The redox potentials of these complexes are outlined in Scheme 1.[2] Chemically the oxidation can be achieved using Ce(IV) ($E^o_{IV/III}$ = 1.7 V at pH = 1.0) [12] or with $[Ru(bpy)_3]^{3+}$ ($E^o_{III/II}$ = 1.2 V). All potentials discussed in this work are reported *vs*. NHE.

In the present context, it is important to note that persulfate acts as an oxidative reagent. Indeed, a 1 mM solution of **Ru^{II}-tda** is slowly oxidized to its Ru(III) species with a 100 mM solution of $S_2O_8^{2-}$ both at pH = 7 and at pH = 1 as shown in Figure 1 and the ESI. On the other hand, under similar conditions **Ru^{IV}-tda** is slowly reduced to Ru(III) at pH = 7, but is stable at pH =1.0 (see SI text and Figure S1 for details).

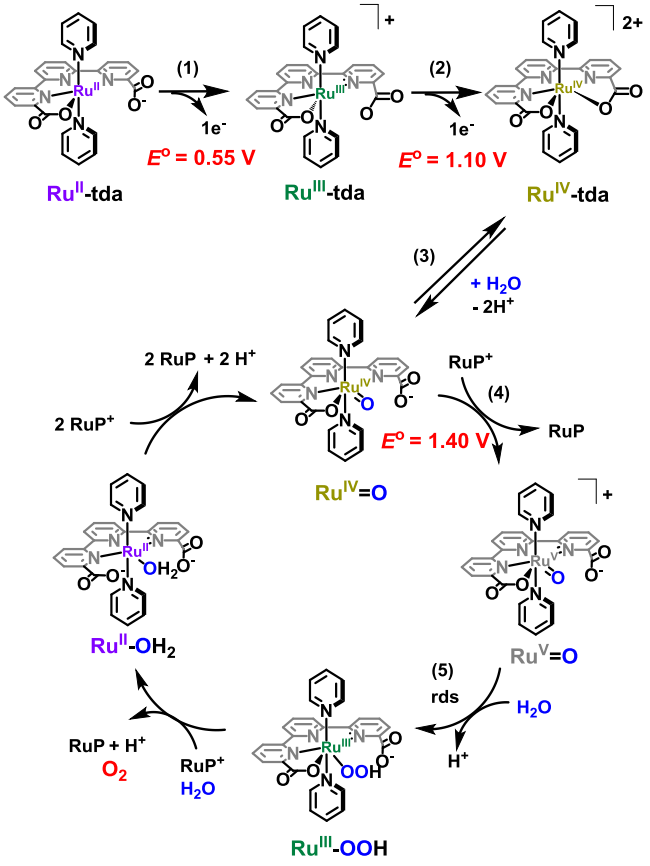

Scheme 1. Ru-tda catalyst precursor at different oxidation sates and simplified catalytic water oxidation cycle proposed for [Ru^{IV}(tda)(py)$_2$(O)], Ru^{IV}=O, at pH = 7.[2]

At pH = 7 the **Ru^{IV}-tda** complex undergoes aquation to generate [Ru^{IV}(tda)(py)$_2$(O)], **Ru^{IV}=O** (see equation 3 in Scheme 1), which is an efficient electrochemical water oxidation catalyst (WOC). This aquation process only takes place at oxidation state IV as has been detailed in our previous publications.[2] The catalytic cycle followed by this complex has been described recently and a simplified reaction sequence is illustrated in Scheme 1.[2] A key step in this cycle is the **Ru^{IV}=O** to **Ru^{V}=O** oxidation, which occurs electrochemically at 1.40 V, followed by O-O bond formation via a water nucleophilic attack (WNA) pathway that generates the corresponding **Ru^{III}OOH**. The latter step has been reported as the rate determining step (rds) of the whole catalytic cycle.[2] A specific feature of this catalytic system is the equilibrium between the catalyst precursor (**Ru-tda**) species and those of the catalyst (**Ru-H$_2$O**) (equation 3, Scheme 1). For the light-driven system reported herein, we found this equilibrium to be a function of the irradiation time (See figure S6 in the SI). After 2 min irradiation, as employed in our transient absorption measurements described below, cyclic voltammetry data indicates that the ratio of **[Ru-H$_2$O]:[Ru-tda]** is 1:50; over long irradiation periods (1 hour) the ratio increases up to 2.6:1 . These results indicate that at pH = 7 under the light-driven catalytic conditions the water molecule is able to coordinate to the metal center and that we can accumulate more aqua species at longer time scales.

In addition, it is important to bear in mind that at pH = 1 the aquation reaction (equation 3, Scheme 1) does not occur and thus at this pH the complex does not show any catalytic activity.[2]

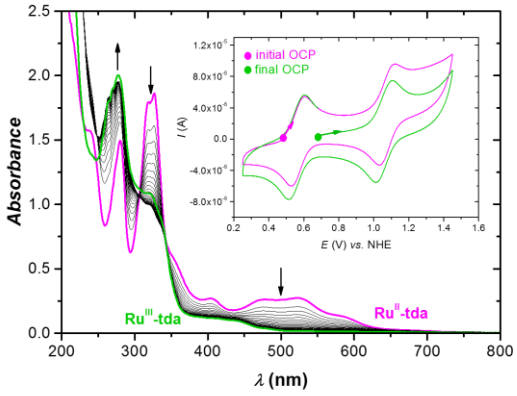

Figure 1. UV-Vis kinetic monitoring for the oxidation of a 4 μM **Ru^{II}-tda** by 10 mM $S_2O_8^{2-}$ in the dark in a 25 mM phosphate buffer aqueous solution, the ionic strength was adjusted at 0.1 M by the addition of Na_2SO_4 . Pink trace, initial spectrum. Green trace final spectrum after 20 consecutive scans measured every 5 s' during 1h. Inset, Cyclic Voltammetry and Open Circuit Potential measured before the addition of persulfate (pink trace) and after 1 hour reaction time (green trace). Scan rate = 100 mV/s. The arrow indicates the scan direction.

Chemically the key oxidation of **Ru^{IV}=O** to **Ru^{V}=O** cannot be accomplished with [Ru^{III}(bpy)$_3$]$^{3+}$ because its III/II redox potential is too low. However the ethyl ester derivative [Ru^{III}(bpy)(bpy-COOEt)$_2$]$^{3+}$ (bpy-COOEt, is 4,4'-ethyl ester dicarboxyalte-2,2'-bipyridine; see Chart 1), **RuP^{+}**, has a E^o = 1.62 V[4a] and thus has sufficient thermodynamic driving force to carry out the redox reaction. Therefore, **RuP^{+}** can potentially be used do drive all the oxidation reactions involved in the catalytic cycle displayed in Scheme 1, and is employed in the study herein.

2.2 Light-Induced water oxidation catalysis

In order to carry out the light-induced water oxidation catalysis we use the **Ru^{IV}=O** species described above as the catalyst (generated in situ from its **Ru^{III}-tda** precursor), driven by **RuP^{+}** generated from **RuP** with light irradiation in the presence of an excess of a sacrificial electron acceptor, such as $S_2O_8^{2-}$. For this purpose the reaction conditions were initially optimized in the absence of catalyst.

2.2.1 Photochemical system optimization in the absence of water oxidation catalyst

Under irradiation conditions in the presence of $S_2O_8^{2-}$, the generation of **RuP^{+}** is described by the equations 1-4 shown in Table 1, where the efficiency definitions are also indicated. A schematic representation of these reactions is

also illustrated in Scheme 2.We optimized this process ($S_2O_8^{2-}$ concentration and ionic strength) based on steady state photoluminescence (PL) experiments following the quenching of the excited stated, **RuP***, by persulfate (see equation 2, Table 1, also Figures S2 and S3 in the SI). This quenching process has been widely studied in the literature for $[Ru(bpy)_3]^{2+}$ [3,6,13,] and is known to be a complex system due to the ionic pairing between the **RuP**$^+$ and the $S_2O_8^{2-}$, which causes a linearity loss in the Stern Volmer plots (see Figure S2b in the SI) associated with a change in ionic strength in the medium.[14] We found optimal reaction conditions at pH = 7, using a 25 mM phosphate buffer (from now on labelled as 7-phbf). These are thus the conditions that will be used throughout the present work unless explicitly mentioned. Under these conditions, a persulfate concentration range of 10-100 mM gives quenching efficiencies ϕ_q of 0.75-0.90 respectively (See Table 1 for efficiency definitions and Fig S2).

Transient absorption spectroscopy was used to investigate the electron transfer kinetics involved in the binary solution of **RuP** dye and $S_2O_8^{2-}$. These processes have been widely studied for the commonly employed $[Ru(bpy)_3]^{2+}$ dye. [3,6,13,15] The change in absorbance of **RuP** in the presence of $S_2O_8^{2-}$ after photoexcitation is characterized by a negative photobleach feature at wavelengths shorter than 600 nm and a positive photoinduced absorbance at the 650-800 nm region (See Figure S3), assigned to the photoinduced generation of **RuP**$^+$, by analogy with $[Ru(bpy)_3]^{2+}$. These transient absorption signals decay with a half-life time ($t_{50\%}$) of 0.7 s, as illustrated at 460 nm in Figure 2 (orange trace) and assigned to decay of photogenerated **RuP**$^+$ species back to its ground state, **RuP**. The raise of these **RuP**$^+$ signals was observed to be biphasic, with an initial instrument response limited (< 150 ns) rise, followed by a slower ($t_{1/2}$ = 3.8 μs) rise, as shown in Figure S4. Following an analogous study by Scandola and coworkers,[7] the initial rise is assigned to the direct oxidation of photogenerated **RuP*** by $S_2O_8^{2-}$ termed "direct oxidation" (eq. 2, Table 1), and the subsequent microsecond phase to diffusion limited oxidation of **RuP** by the radical $SO_4^{\cdot-}$ to generate again **RuP**$^+$, named "dark oxidation" (eq. 3, Table 1 and Scheme 2). The efficiency of the dark oxidation relative to the preceding direct oxidation can be estimated from the relative amplitudes of these two phases, giving a value of ϕ_d = 0.6,[3,7] (see Table 1 for details). The combination of these Transient Absorption Spectroscopy (TAS) and PL experiments allow to calculate an overall quantum efficiency for the **RuP**$^+$ generation, ϕ_{RuP+} = 0.56, that considers both the direct and dark processes (see Table 1 for definition), corresponding to the generation of 1.12 **RuP**$^+$ species per absorbed photon.

Table 1. Efficiencies of Light and Dark Reactions Studied.

Process	Chemical Reaction	Effiency Definition.
Light absorption:	RuP + hυ -> RuP* (1)	
Direct generation of **RuP**$^+$:	RuP* + $S_2O_8^{2-}$ -> RuP$^+$ + SO_4^{2-} + $SO_4^{\cdot-}$ (2)	$\phi_q = 1 - I/I_o$ [a]
Dark generation of **RuP**$^+$:	RuP + $SO_4^{\cdot-}$ -> RuP$^+$ + SO_4^{2-} (3)	$\phi_d = \frac{\Delta O.D._d}{\Delta O.D._l}$ [b]
Overall rxs (1)-(3)	2 RuP + hυ + $S_2O_8^{2-}$ -> 2RuP$^+$ + 2 SO_4^{2-} (4)	$\phi_{RuP+} = \frac{1}{2}\{\phi_q(1+\phi_d)\}$
Bimolecular electron transfer	RuP$^+$ + Ru^{IV}=O -> RuP + Ru^{V}=O (5)	$\phi_{ET} = 1 - \frac{k_0}{k_{obs}}$ [c]
Measured oxygen quantum yield	hν 2 H_2O --------> O_2 + 4H$^+$ + 4e$^-$ (6)	$\phi_{O2} = \frac{2 \times (O_2\ molecules)_t}{Absorbed\ photons \times \Delta t \times Area}\ x\ 100\%$ [d]
Calculated oxygen Quantum yield		$\phi_{Total} = \phi_{RuP+} * \phi_{ET} * \phi_{Cat}$ [e]

[a] I and I_o are the photoluminescence intensities in the presence and absence of $S_2O_8^{2-}$ respectively.

[b] From TAS decays probed at 460 nm in the absence of catalyst: $\Delta O.D._l$, is the amplitude of the initial phase of the decay probed at 460 nm. $\Delta O.D._d$, is the amplitude of the second phase (see Figure S4).[12]

[c] From TAS decays probed at 460 nm with different catalyst concentrations: $k_o = 1/t_{50\%}$ without Catalyst and $k_{obs} = 1/t_{50\%}$ in the presence of catalyst.

[d] This calculation assumes an ideal quantum efficiency of 2 photons per molecule of oxygen, accounting for the ideal generation of two **RuP**$^+$ per photon and four **RuP**$^+$ per oxygen molecule.

[e] ϕ_{Cat} is the chemical efficiency of water oxidation by the catalyst, assumed herein to correspond to the Faradaic efficiency measured under electrochemical oxidation.

2.2.2 System optimization in the presence of the water oxidation catalyst

Once the combination of **RuP** dye and sacrificial electron acceptor had been optimized and the main kinetic and spectroscopic parameters unveiled for this binary system, the next step involved the addition of the water oxidation catalyst into the system.

Figure 3 shows that, in the absence of persulphate, the emission spectrum of a 4 μM **RuP** is not quenched by the addition of 4 μM of the catalyst precursor **Ru^{II}-tda** in a 7-phbf solution (orange). However, when a solution of 10 mM persulfate is added to the **RuP** / **Ru^{II}-tda** solution, the emission is quenched by 60%, approximately independent of the catalyst concentration (ϕ_q as a function of $[S_2O_8^{2-}]$ in the presence of catalyst is presented in Figure S5). We find that under identical conditions (Compare Figure S2a and S5 in the SI) in the absence of **Ru^{II}-tda**, the quenching yield is ϕ_q = 0.75, indicating that in the former case the presence of the Ru catalyst reduces the efficiency of the electron scavenging, possibly due to additional deactivation pathways. With ϕ_q = 0.60 in the presence of the catalyst and the sacrificial agent, then the overall quenching efficiency for the generation of **RuP^{+}** is, ϕ_{RuP+} = 0.50 (i.e.: one **RuP^{+}** per photon absorbed).

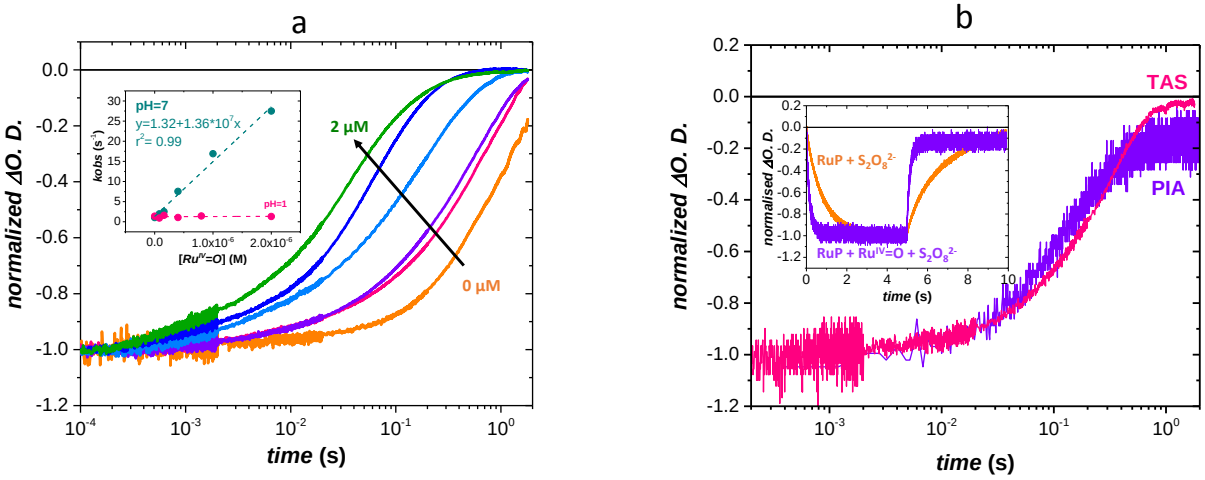

Figure 2. a, Normalized TA decays probed at 460 nm (λ_{ex} = 500 nm; laser intensity = 177.48 μJ cm^{-2}) for a 7-phbf solution **RuP** (20 μM), $S_2O_8^{2-}$ (10 mM) in the absence of catalyst (orange trace) and with different **[Ru^{IV}=O]** (pink, 80 nM; violet, 160 nM; light blue, 0.4 μM; dark blue, 1 μM, green 2 μM) that were generated from the corresponding **[Ru-tda]** precursors (see text). Data collected under N_2 at 10 μs-2 s timescales. Inset, plot of k_{obs} *vs.* **[Ru^{IV}=O]** at pH = 7 and pH -= 1**.**

b, TAS decays measured at 460 nm under pulsed laser (pink) and 5 s LED irradiation (15.4 mW cm^{-2}) (violet). Data shown for a 20 μM **RuP**, 10 mM $Na_2S_2O_8$ and 40 μM **Ru^{II}-tda** solution that generates a **[Ru^{IV}=O]** = 0.8 μM. Inset, full linear timescale traces of the transient signal under LED excitation showing the change of both at light on and light off, in the absence (orange) and presence of 0.8 μM **Ru^{IV}=O** (violet).

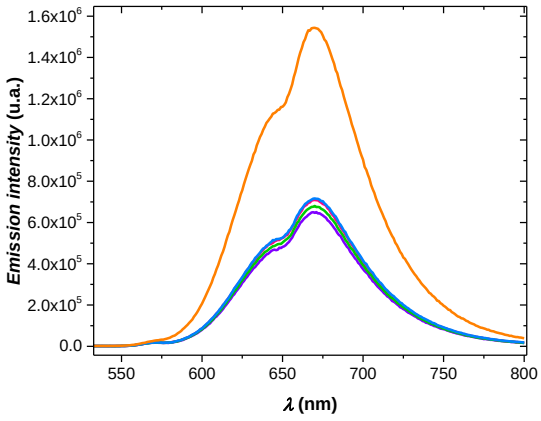

Figure 3. Emission spectra of a 4 μM **RuP** and 4 μM **Ru^{II}-tda** solution (orange) in the absence of a sacrificial electron acceptor. Emission spectra of **RuP** (4 μM), $Na_2S_2O_8$ (10 mM) and different **Ru^{II}-tda** concentrations (violet, 2 μM; pink, 4 μM; green, 6 μM; blue, 8 μM) all in a 7-phbf solution.

2.2.3 Kinetic characterization of the light-induced reaction between the catalyst and the dye with the complete system.

Transient absorption spectroscopic measurements with the complete system involving the dye, the sacrificial electron acceptor and the water oxidation catalyst were carried out in order to investigate the kinetic processes involved. All TAS measurements were performed after a 2 minute sample irradiation in order to equilibrate all the species in solution and thus measured under steady state catalytic conditions. Under these conditions, the catalyst precursor equilibrates with the active catalytic species (see equation 3 in Scheme 1). The relative concentrations were estimated to be 50:1 **Ru^{IV}-tda:Ru^{IV}=O** , after 2 minute irradiation, as discussed above (see Figure S6 in the SI). The kinetic analysis shown in Figure 2a inset supports the extrapolation of this ratio at different precursor concentrations. However

with low intensity irradiation the catalyst concentration might be even lower.

Figure 2a shows the **RuP**$^{+}$ bleach signal decay kinetics at 460 nm in the presence of $Na_2S_2O_8$ as a function of catalyst precursor **Ru^{II}-tda** concentration in a 7-phbf solution. The decay kinetics observed in the TAS experiments correspond to the slowest ET transfer step (equation 4, Scheme 1), that is a bimolecular interaction between **Ru^{IV}=O** and **RuP**$^{+}$. As shown in Figure 2, the decay kinetics accelerate with increasing the catalyst's concentration. The half-times of these decays fitted well with a simple bimolecular expression with a reaction time linearly dependent on the catalyst concentration. This is in agreement with a pseudo-first order behavior where the [**Ru^{IV}=O**] >> [**RuP**$^{+}$], and thus k_{ET} can be extracted from the plot of k_{obs} *vs.* [**Ru^{IV}=O**] as shown in the inset of Figure 2 and described in equations 5a-5c).

$$v = k_{ET}\,[Ru^{IV}{=}O][RuP^{+}] \quad (5a)$$

$$[Ru^{IV}{=}O] >> [RuP^{+}];\ k_{obs} = k_{ET}[Ru^{IV}{=}O] \quad (5b)$$

$$v = k_{obs}[RuP^{+}] \quad (5c)$$

The calculated electron transfer constant is $k_{ET} = 1.4{\cdot}10^{7}$ $M^{-1}\,s^{-1}$. Further evidence that confirms the pseudo-first order nature of the reaction comes from the transient absorption decays using laser intensities of 180 and 20 μJ/cm^2 (Figure 4). These experiments generate different concentrations of **RuP**$^{+}$ depending on the energy used but the normalized bleach kinetics is independent of [**RuP**$^{+}$], consistent with the pseudo-first order behavior indicated in the suite of equations 5a-5c.

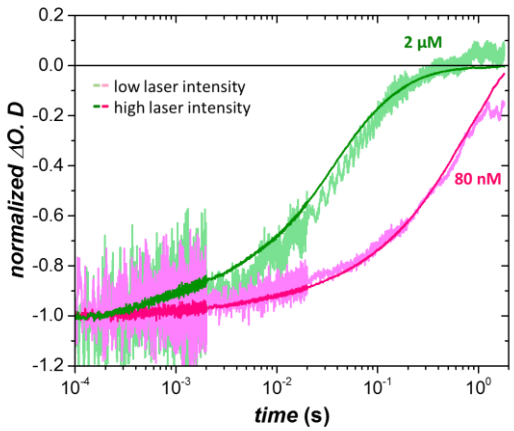

Figure 4. Normalized transient absorption decays at 460 nm of a 20 μM **RuP**, 10 mM $Na_2S_2O_8$ solution (7-phbf), containing two **Ru^{IV}=O** concentrations (violet, 80 nM; green, 2 μM) in a 7-phbf solution. Data collected under N_2 at a 10 μs-2 s timescale after dye excitation (λ_{ex} = 500 nm), using two different laser intensities of 180 (dark line) and 20 (light line) μJ cm^{-2}.

We next estimate the quantum efficiency of the oxidation of **Ru^{IV}=O** by **RuP**$^{+}$. This, ϕ_{ET}, can be estimated from the acceleration of the **RuP**$^{+}$ bleach decays (Figure 2a) at different catalyst concentrations (see Table 1). Such analysis gives ϕ_{ET} values that range from of 0.45 at initial 4 μM **Ru^{II}-tda** to an impressive 0.96 at 100 μM as is discussed further below.

Photoinduced Absorbance (PIA) experiments were undertaken on the same ternary system at pH = 7 employed in Figure 2a, using quasi-steady state irradiation achieved by 5 s 365 nm LED (light emitting diode) excitation pulses; the results are shown in Figure 2b. The inset shows full time traces measuring the **RuP**$^{+}$ bleach signal in the presence and absence of **Ru^{IV}=O**. In the absence of catalyst, a **RuP**$^{+}$ bleach signal is observed, with a rise and fall times of ~ 1 s ($t_{50\%}$), assigned to the accumulation of oxidized **RuP**$^{+}$ under these quasi steady state conditions. The rise and fall times ($t_{50\%}$) of ~ 1s are consistent with the **RuP**$^{+}$ lifetime observed under laser excitation in the absence of catalyst with TAS measurements (Figure 2a). In the presence of the **Ru^{IV}=O** catalyst, the LED irradiation resulted in a faster **RuP**$^{+}$ bleach rise and decay due to electron transfer between the dye and catalyst. The decay kinetics of the **RuP**$^{+}$ bleach signal, monitored when the LED is turned off, and assigned to the oxidation of **Ru^{IV}=O** under these quasi-steady state conditions, are shown in the main part of Figure 2b (violet trace) and are strikingly similar to those one obtained under short pulse laser excitation (pink trace). These experiments support our previous assumption that the TAS experiments are indeed already under steady state conditions. In addition, a similar PIA experiment was carried out using a Clark electrode to simultaneous measure the formation of O_2, further confirming the mentioned steady state equilibrium (see Figure S7).

Similar experiments were carried out at pH = 1, where the aquation reaction (reaction 3, Scheme 1) does not occur. At this pH and under steady state conditions the catalyst precursor is oxidized to its higher oxidation states **Ru^{IV}-tda** but no further reactions occur because no catalytic species can be generated.[2] In agreement with this, the TAS kinetics of the bleach (k_{obs}) were observed to be independent of the catalyst precursor concentration, as can be observed in the inset of Figure 2a (see also Figure S9). This is a key result that further supports our discussion above that at pH = 1, light irradiation (such as the 2 minute light equilibration time employed prior to our TAS measurements) results in the initial catalyst precursor at oxidation state II being completely driven to its oxidation state IV species **Ru^{IV}-tda**, with this species being unable to undergo further oxidation by **RuP**$^{+}$.

2.3 Light-driven O_2 generation

With the above-described quasi-steady state irradiation conditions, we were in a position to design steady state experiments for light-induced water oxidation using **RuP** as photosensitizer, **Ru^{II}-tda** as a water oxidation catalyst precursor and persulfate as sacrificial electron acceptor in a 7-phbf solution. Figure 5a shows the oxygen evolution profiles as a function of time during one hour of irradiation, measured with a gas phase Clark electrode, for different **Ru-tda** concentrations ranging from 1-90 μM in the presence of 10 mM persulfate and 200 μM **RuP** at 7-phbf.

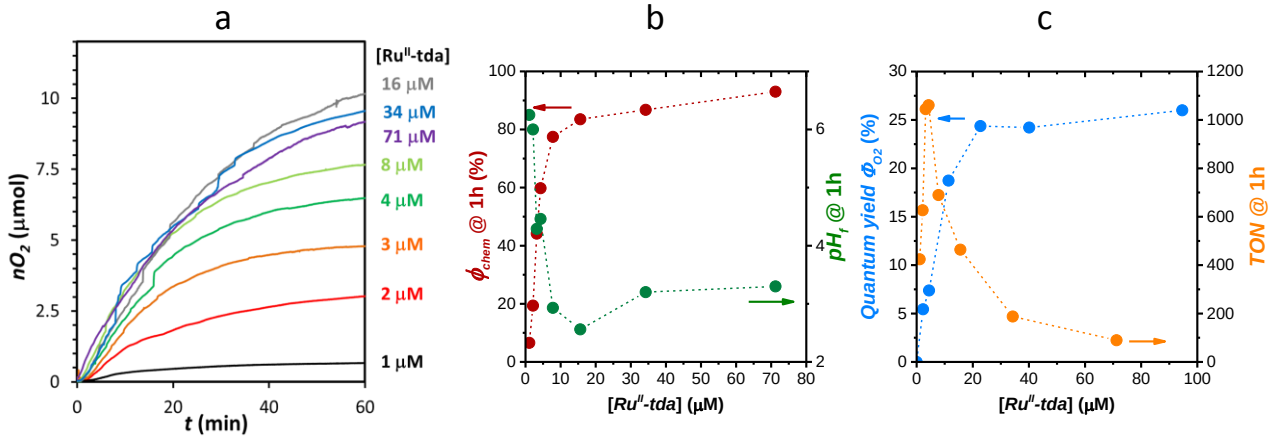

Figure 5. Bulk oxygen evolution experiments measured in the gas phase during 1 h irradiation (1 sun) at different [**Ru^{II}-tda**] (black, 1 μM; red, 2 μM; orange, 3 μM; dark green, 4 μM; light green, 8 μM; grey, 16 μM; blue, 34 μM, violet, 71 μM) containing the following $Na_2S_2O_8$ concentration: black, 9.9 mM; red 9.9 mM; orange, 10.9 mM; dark green, 10.9 mM; light green, 9.9 mM, grey, 12.4 mM; blue, 10.7 mM and violet, 10 mM and 0.2 mM **RuP** in a 2 mL 7-phbf solution. (a) Oxygen evolution *vs*. time. (b) Chemical efficiency (red) and final pH_f (green) *vs*. [**Ru^{II}-tda**] that after one hour irradiation is partially converted to the catalyst giving a final ratio [**Ru^{IV}=O**]/[**Ru^{II}-tda**] = 2.5, see SI. (c) Initial Quantum yield (ϕ_{O_2}) (turquoise) and TONs (orange) based on the final [**Ru^{IV}-=O**].

Figure 5b shows a plot of the chemical efficiency, ϕ_{Chem}, defined as (2 x moles of oxygen generated/ moles of persulfate added) x 100. It is interesting to see how increasing the concentration of **Ru^{II}-tda** from 1 to 16 μM ϕ_{Chem} also increases from 7 to 80%. Upon further increase of **Ru^{II}-tda** concentration, the chemical efficiency levels off reaching about 93% at 90 μM. This result shows that for this system at high catalyst concentrations, the overall amount of oxygen generated is limited only by the amount of sacrificial electron donor added to the solution, confirming the high efficiency and stability of the catalyst under the present conditions. Indeed it is also impressive to see that the system achieves a value of 1050 turnovers per hour with a 4 μM **Ru^{II}-tda** (3 μM **Ru^{IV}=O**) concentration, ranking amongst the most efficient light-induced molecular water oxidation catalysts reported (Figure 5c).[3-4,6-11]

The low chemical efficiency at low catalyst concentrations is consistent with the lower quantum efficiency for the oxidation of the catalyst by **RuP^{+}** (ϕ_{ET}) determined from our transient absorption data above, and indicates that competing deactivation pathways become important. The main deactivation processes for **RuP^{+}** are likely to be associated with the oxidation of the bpy ligand of the **RuP** dye by the **RuP^{+}** species as well as by the radical $SO_4^{\bullet-}$ species, as has been previously proposed for related systems.[15] These deactivation pathways also result in significant dye degradation, apparent from progressive photobleaching of the dye optical absorption, which was most pronounced at low catalyst concentrations. (see Figure S11 in the SI).[4a,15]

During the light-driven catalytic experiments, as oxygen is released four protons are generated per molecule of oxygen and even under a buffered solution the pH significantly decreases, as shown in Figure 5b. The pH decrease can alter the rates of electron transfer, which will probably be slower at lower pH due to the decrease in energetic driving force,[2] as well as changing the equilibrium of equation 3 (Scheme 1) that is responsible for the generation of the active species. Therefore, it can significantly influence the delicate balance among the different chemical reactions involved in this complex process. The addition of alkali to reverse this pH change would result in a significant increase in ionic strength of the system, which will also decrease the **RuP^{+}** generation efficiency, thus preventing efficientrecycling of the system.

Quantum efficiencies for oxygen generation (ϕ_{O_2}) were calculated based on the initial rates of oxygen formation and the density of photons absorbed per second as indicated in Table 1 and the SI, and displayed in Figure 5c as a function of catalyst precursor concentration. As can be observed in Figure 5c, ϕ_{O_2} increases with increasing [**Ru^{II}-tda**] and closely parallels that of ϕ_{Chem}. However while for the latter we reach values close to 100%, for the former it levels off at approximately 25% for 20 μM **Ru^{II}-tda**; this photon to oxygen quantum efficiency still constitutes the highest efficiency reported to date for this type of molecular light-driven water oxidation systems. We note that our calculation of ϕ_{O_2} assumes, conservatively, that each absorbed photon can optimally generate two **RuP^{+}** and therefore that ϕ_{O_2} = 100 % would correspond to one molecule of O_2 per two photons. The factors still limiting this impressive quantum efficiency will be discussed below.

3. DISCUSSION

We have demonstrated that the proper combination of a dye, **RuP^{+}**, a water oxidation catalyst, **Ru^{IV}=O,** and persulfate as sacrificial electron acceptor can constitute a light-driven system with unprecedentedly high chemical (ϕ_{Chem} = 96%) and quantum (ϕ_{O_2} = 25%) efficiencies, for the light-induced oxidation of water to molecular oxygen. This is

achieved thanks primarily to the high stability and extremely fast water oxidation kinetics associated with the **Ru^{IV}=O** catalyst. The latter is generated in situ from the **Ru^{II}-tda** catalyst precursor under irradiation. Both catalyst and catalyst precursor remain in equilibrium during the steady state oxygen formation under which the transient absorption spectroscopic measurements are carried out in the present work. Under these conditions we measure the rate constant for electron transfer from **RuP^{+}** to **Ru^{IV}=O** to be k_{ET} = 1.4·10^{7} M^{-1} s^{-1}. This rate constant is obtained based on a simple kinetic model assuming a pseudo-first order regime where [**RuP^{+}**] << [**Ru^{IV}=O**]. This is further corroborated by identical kinetic decay of samples irradiated with lasers of different intensity (See Figure 4). Similar kinetics were also obtained from quasi-steady state irradiation conditions (Figure 2b). Finally an indirect additional support is obtained based on the unchanged kinetics at pH = 1 with different catalyst concentrations, pH conditions under which the catalyst is trapped in its inactive **Ru^{IV}-tda** state. The value of k_{ET} obtained for our system is one to two orders of magnitude slower than for related systems with polyoxometalate complexes reported in the literature,[3,7a,8] However in these cases there was no proof of oxygen formation during the time scale of the measurements and therefore they may be related to the oxidation of an intermediate at low oxidation states, that are known to be much faster.[16]

Scheme 2 summarizes the main reactions occurring in the present system including the kinetics of each individual step. Once the **RuP*** is generated, all the main productive process involved in the generation of O_2 occur within the time scale of ns to ms, including oxidation of the water oxidation catalyst. This molecular water oxidation catalyst exhibits both exceptional stability and the potential to drive water oxidation with a TOF of up to 8,000 s^{-1}. These very favorable light-driven kinetics and catalyst characteristics are presumably responsible for the record high quantum yields obtained.

The quantum efficiency for oxygen evolution ϕ_{O_2} corresponds to the efficiency with which our light-driven systems utilizes absorbed photons to drive water oxidation, and is therefore a key measure of the efficiencies of the molecular processes determining system function. The three main processes involved in this light-driven catalytic function, as depicted in scheme 2, correspond to: (1) **RuP^{+}** generation with a quantum efficiency of ϕ_{RuP+} (determined per 0.5 absorbed photons, as discussed above), (2) electron transfer between **RuP^{+}** and **Ru^{IV}=O** under constant illumination, with a quantum efficiency of ϕ_{ET} and (3) water oxidation by the oxidized catalyst to yield molecular oxygen generation, with an efficiency of ϕ_{CAT}. The efficiencies ϕ_{RuP+} and ϕ_{ET} , determined from our kinetic analyses above, are plotted in Figure 6 as a function of **Ru^{II}-tda** concentration. For ϕ_{CAT}, we assume a value of 92%, determined from the faradaic efficiency of this catalyst under electrocatalytic system (see further discussion below).[2] This figure also includes a plot of the overall system quantum efficiency calculated from these three separate efficiencies: $\phi_{TOTAL} = \phi_{RuP+} * \phi_{ET} * \phi_{CAT}$ as well as the directly measured quantum efficiency for oxygen evolution ϕ_{O_2}. The near unity value of this Faradaic efficiency is further supported by our high chemical efficiency (93%) measured under light-driven catalytic operation. It is apparent from Figure 6 that the quantum yields of oxygen evolution measured directly from oxygen concentration measurements (ϕ_{O_2}) show similar behaviour to those calculated from our kinetic analyses (ϕ_{TOTAL}). Our calculated maximal quantum yield is in reasonable agreement with our measured one, differing by 18 % (we discuss the origin of this difference below). As such we can conclude that the kinetic data and analysis we report herein are indeed able to determine the main factors limiting the quantum efficiency of our light-driven system.

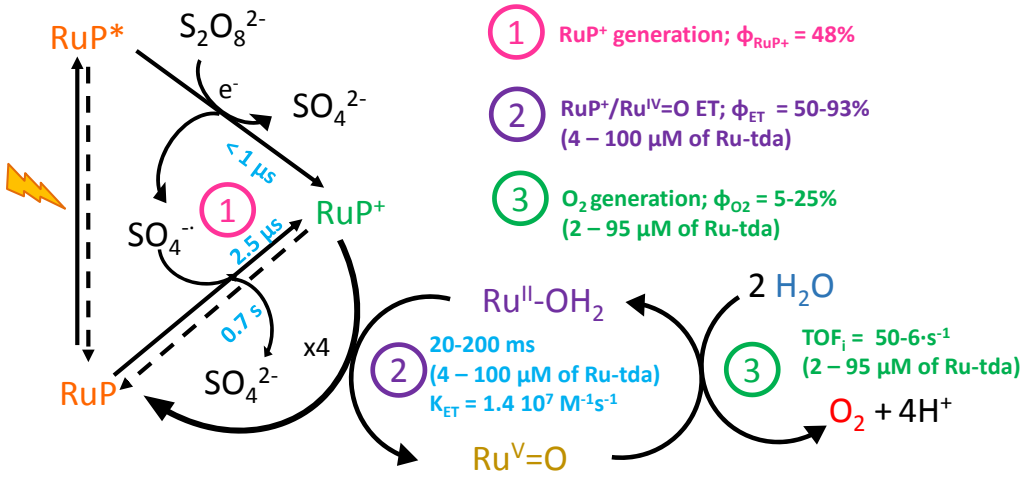

Scheme 2. Main processes and their time scales involved in the oxygen evolution reaction involving the RuP dye, the Ru^{IV}=O water oxidation catalyst and persulfate as sacrificial electron acceptor in a 7-phbf solution. (1) RuP^{+} photogeneration. (2) Electron transfer between RuP^{+} and the Ru^{IV}=O catalyst. (3) Initial dioxygen generation from water in the photoactivated system.

As has been discussed above, the measured quantum yield of O_2 (ϕ_{O2}) depends on the catalyst concentration (light blue trace Figure 6). We can assign this dependency to the increased efficiency of electron transfer between **RuP**$^+$ and **Ru^{IV}=O** with increasing catalyst concentration. (Compare violet trace with light and dark blue lines, Figure 6). This is related to the bimolecular nature of the process, with increasing the catalyst concentration enhancing the probability that **RuP**$^+$ species will oxidize a catalyst molecule rather than alternative oxidation substrates. This phenomena has been previously reported, but, the instability of the catalyst at high concentrations prevented the achievement of high efficiencies.[3,6b,8b,9] In the literature there are other examples showing that enhancement of the interaction between the dye and the catalyst increases the quantum yields by favouring the dye-catalyst electron transfer.[5,6a, 8a,10]. In our system the stability of the **RuP** sensitizer is also improved by increased catalyst concentration (Figure S11). The susceptibility of **RuP** to irreversible decomposition in its oxidized state has been reported previously, and is most likely associated with secondary oxidations of the bpy ligands.[15] It is striking that for the light-driven system reported herein, the system stability is not limited by catalyst degradation but rather by the degradation of the sensitizer, as well as the increase in ionic strength and proton concentration during operation.

It is also apparent from Figure 6 that the largest quantum efficiency loss (~ 50 %) results from inefficient generation of **RuP**$^+$ by the sacrificial electron donor $S_2O_8^{2-}$ (ϕ_{RuP+}). Whereas in principle this sensitizer/donor system should yield two **RuP**$^+$ per photon, in practice inefficiencies in both oxidation reactions result in only 0.98 **RuP**$^+$ per photon. We expected to enhance this efficiency by increasing the concentration of $S_2O_8^{2-}$, but lower oxygen yields were measured, assigned to the resulting higher ionic strength and/or lower pH, reducing the efficiency of catalyst oxidation by **RuP**$^+$. Furthermore, at low catalyst concentrations, additional quantum efficiency losses result from the inefficient catalyst oxidation by **RuP**$^+$ (ϕ_{ET}).Remarkably, the efficiency of this photoactivated system for oxygen generation is not limited by the activity of the catalyst, whereas by the photon flux and the generation of the **RuP**$^+$. This analysis therefore clearly identifies that further advances in system performance will require focus on the development of the sensitizer and sacrificial electron donor systems, rather than on the improvement of the catalyst turn over frequency.

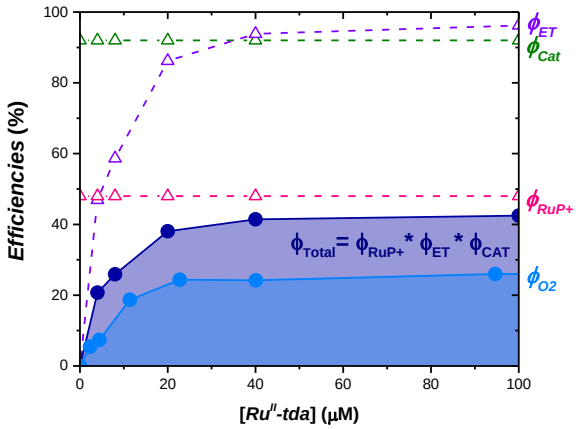

Figure 6. Summary of the efficiencies of the light-driven system as a function of **[Ru^{II}-tda].** Dashed lines represent the estimated efficiencies for the individual processes: **RuP**$^+$ generation (ϕ_{RuP+}) (pink); Electron transfer between **RuP**$^+$ and **Ru^{IV}=O** accumulated in the steady state of the catalytic cycle (ϕ_{ET}) (violet); Faradaic efficiency of **Ru^{IV}=O** under electrocatalytic conditions (ϕ_{CAT}) (green). Solid lines indicate the quantum yield efficiency estimated from: bulk oxygen generation (ϕ_{O2}) (light blue) and from spectroscopic experiments (Φ_{TOTAL}) (dark blue).

The above discussion has focused on the chemical and quantum efficiencies of our light-driven system. We now turn to consider the rate of oxygen evolution. Whilst the **Ru^{IV}=O** WOC is capable of a TOF of 8,000 s^{-1} when driven electrochemically, in the light-driven system reported herein, the light-driven TOF is in the range of 6 - 50 s^{-1} (determined as moles of oxygen per second / moles of **Ru^{IV}=O**. The light-driven catalytic TOF increases upon lowering the concentration of the catalyst, indicating that it is not limited by the **Ru^{IV}=O** WOC performance. Rather it will be determined by the flux of photons absorbed by the system, and by the quantum yield associated with the use of the absorbed photons to drive water oxidation. Under one sun irradiation, the absorbed photon flux is 0.17 μmoles s^{-1}. Using the value for ϕ_{TOTAL} determined above under conditions of maximal oxygen evolution rate (40 μM of **Ru^{II}-tda** added, corresponding to 1.6 nmoles **Ru^{IV}=O**), this absorbed photon flux should results in a TOF of 22 s^{-1}, compared to a measured TOF under these conditions of 13 s^{-1}. These calculations confirm that the final performance is mainly determined by the absorbed photon flux, with the difference between our measured and calculated TOF's indicating an additional loss pathway.

There is an additional efficiency loss not accounted for by our kinetic analysis; this most probably results from the different conditions, **RuP**$^+$ concentration and **Ru^{IV}=O** / **RuP**$^+$ / $S_2O_8^{2-}$ ratio, employed for our spectroscopic and bulk oxygen measurements. These differences could mainly effect the efficiencies related with the oxidized dye generation (ϕ_{RUP+})and the electron transfer between the **RuP**$^+$ and the **Ru^{IV}=O** (ϕ_{ET}). The dependency of light-

driven catalytic quantum yield upon **Ru^{II}-tda** concentration estimated from O_2 bulk and from spectroscopic measurements, suggests that the most inefficient process is the oxidized dye generation (ϕ_{RUP+}).

The absorbed photon flux limitation we observe herein reflects the limited light harvesting capability of our light-driven system. We note that increasing the concentration of the sensitizer will not substantially improve this, as over the spectral range of absorption of the sensitizer, almost all photons are absorbed. The ratio of sensitizer per catalyst can be improved by lowering the catalyst concentration, but at the expense of lowering ϕ_{ET}, the efficiency of electron transfer from the oxidized sensitizer to the catalyst. This light harvesting limitation is addressed in photosynthetic organisms by the assembly of large antenna complexes (100's of molecular light absorbers) funneling excitation energy into each catalytic site. Our observation that the effective TOF of our light-driven system is limited primarily by light harvesting efficiency is further evidence of the high performance of the molecular water oxidation catalyst employed herein.

4. CONCLUSIONS:

Herein we have reported a remarkably efficient molecular light-driven system for oxidation of water to oxygen and have undertaken a kinetic analysis of the factors determining the efficiency of this system. At high concentrations of catalyst, the system operates with a quantum yield of 25% and a chemical efficiency of 93 %, the highest reported to date for this type of light-driven system, attributed primarily to favorable electron transfer and oxygen evolution kinetics. A high catalyst concentration is found to be required to optimize the efficiency of electron transfer between the oxidized sensitizer and the catalyst, which also has the effect of improving sensitizer stability. The main limitation to the light-driven system quantum efficiency is found to be the relatively low efficiency of $S_2O_8^{2-}$ as an electron scavenger to oxidize **RuP*** to **RuP$^+$** , mainly due to the competing relaxation back to the **RuP** ground state. The overall rate of light-driven oxygen generation is found to be determined primarily by the incident photon flux. The **Ru^{IV}=O** catalyst is found to be so robust and fast that neither the system efficiency nor lifetime are limited by its performance. As such we conclude that the performance of this remarkably efficient light-driven oxygen production system is limited not by the properties of the catalyst, but rather by the sensitizer and electron scavenger properties and by the incident photon flux.

AUTHOR INFORMATION

Corresponding Author

*lfrancas@ic.ac.uk.

*allobet@iciq.cat

Present Addresses

¶ Molecular Biophysics and Integrated Bioimaging Division, Lawrence Berkeley National Laboratory, One Cyclotron Road, Berkeley, California 94720, USA

ξ Department of Chemical and Pharmaceutical Sciences, University of Ferrara, Via Fossato di Mortara 17-19, 44100 Ferrara, Italy

Notes

The authors declare no competing financial interests

ASSOCIATED CONTENT

Supporting Information.

Experimental details, calculations of quantum yields, efficiencies and TOF. Additional UV-VIS, Cyclic voltammetries, quenching efficiencies, Transient Absorption Spectrocopy spectra and decays, Photoinduced Spectrocopy decays and oxygen detection measurements. All this information is available free of charge on the ACS Publications website.

ACKNOWLEDGMENT

We acknowledge financial support from the European Research Council (project Intersolar 291482), L.F. thanks the EU for a Marie Curie fellowship (658270) and Cost Action CM1202. E.P. thanks the EPRSC for a DTP scholarship. A.R. thanks the Royal Society of Chemistry for a Research Fund Grant (RF17-3475). R.M thanks "La Caixa" foundation for a PhD scholarship. Financial support from MINECO and FEDER (CTQ-2016-80058-R, CTQ2015-64261-R, CTQ-2014-52974-REDC, SEV-2013-0319) is also gratefully acknowledged.

REFERENCES

[1] (a) Tong, L.; Thummel, R. P. *Chem. Sci.* **2016,** *7*, 6591-6603. (b) Yamamoto, M.; Tanaka, K. *ChemPlusChem* **2016,** 81, 1028-1044. (c) Sander, A. C.; Maji, S.; Francàs, L.; Böhnisch, T.; Dechert, S.; Llobet, A.; Meyer, F. *ChemSusChem* **2015,** 8, 1697-1702. (d) Garrido-Barros, P.; Funes-Ardoiz, I.; Drouet, S.; Benet-Buchholz, J.; Maseras, F.; Llobet, A. *J. Am. Chem. Soc.* **2015**, 137, 6758-6761. (e) J. D. Blakemore, R. H. Crabtree and G. W. Brudvig, *Chem. Rev.* **2015**, 115, 12974-13005 (f) Neudeck, S.; Maji, S.; López, I.; Meyer, S.; Meyer, F.; Llobet, A. *J. Am. Chem. Soc.* **2014,** 136, 24-27. (g) Llobet, A. *Molecular Water Oxidation Catalysis: A Key Topic for New Sustainable Energy Conversion Scheme*, 1st Edition, John Wiley & Sons, Chichester, 2014. (h) Kärkäs, M. D.; Verho, O.; Johnston, E. V.; Åkermark, B. *Chem. Rev.* **2014**, 114, 11863-12001.

[2] Matheu, R.; Ertem, M. Z.; Benet-Buchholz, J.; Coronado, E.; Batista, V. S.; Sala, X.; Llobet, A., *J. Am. Chem. Soc.* **2015,** 137, 10786-10795.

[3] Lewandowska-Andralojc, A.; Polyansky, D. E.; Zong, R.; Thummel, R. P.; Fujita, E. *Phys. Chem. Chem. Phys.* **2013,** 15, 14058-14068.

[4] (a) Berardi, S.; Francàs, L.; Neudeck, S.; Maji, S.; Benet-Buchholz, J.; Meyer, F.; Llobet, A. *ChemSusChem* **2015,** 8, 3688-3696. (b) Xu, Y.; Fischer, A.; Duan, L.; Tong, L.; Gabrielsson, E.; Åkermark, B.; Sun, L., *Angew. Chem. Int. Ed.* **2010,** 49, 8934-8937. (c) Roeser, S.; Farràs, P.; Bozoglian, F.; Martínez-Belmonte, M.; Benet-Buchholz, J.; Llobet, A. *ChemSusChem* **2011,** 4, 197-207.(d) Laine, T. M.; Karkas, M. D.; Liao, R.-Z.; Akermark, T.; Lee, B.-L.; Karlsson, E. A.; Siegbahn, P. E. M.; Akermark, B. *Chem. Commun.* **2015,** 51, 1862-1865. (e) Wang, L.; Duan, L.; Tong, L.; Sun, L. *J. Catal.* **2013,** 306, 129-132.(f) Tong, L.; Wang, Y.; Duan, L.; Xu, Y.; Cheng, X.; Fischer, A.; Ahlquist, M. S. G.; Sun, L. *Inorg. Chem.* **2012,** 51, 3388-3398. (g) Kärkäs, M. D.; Åkermark, T.; Johnston, E. V.; Karim, S. R.; Laine, T. M.; Lee, B.-L.; Åkermark, T.; Privalov, T.; Åkermark, B. *Angew. Chem. Int. Ed*. **2012**, 51, 11589-11593.(h) Karlsson, E. A.; Lee, B.-L.; Åkermark, T.; Johnston, E. V.; Kärkäs, M. D.; Sun, J.; Hansson, Ö.; Bäckvall, J.-E.; Åkermark, B. *Angew. Chem. Int. Ed.* **2011,** 50, 11715-11718. (i) Xu, Y.; Fischer, A.; Duan, L.; Tong, L.; Gabrielsson, E.; Åkermark, B.; Sun, L. *Angew. Chem. Int. Ed.* **2010,** 49, 8934-8937. (j) Xu, Y.; Duan, L.; Tong, L.; Akermark, B.; Sun, L., *Chem. Commun.* **2010,** 46, 6506-6508. (k) Duan, L.; Xu, Y.; Gorlov, M.; Tong, L.; Andersson, S.; Sun, L. *Chem. Eur. J.* **2010,** 16, 4659-4668. (l) Besson, C.; Huang, Z.; Geletii, Y. V.; Lense, S.; Hardcastle, K. I.; Musaev, D. G.; Lian, T.; Proust, A.; Hill, C. L. *Chem. Commun.* **2010,** 46, 2784-2786. (m) Duan, L.; Xu, Y.; Zhang, P.; Wang, M.; Sun, L. *Inorg. Chem.* **2010,** 49, 209-215.

[5] Li, H.; Li, F.; Zhang, B.; Zhou, X.; Yu, F.; Sun, L. *J. Am. Chem. Soc.* **2015,** 137, 4332-4335.

[6] (a) Geletii, Y. V.; Huang, Z.; Hou, Y.; Musaev, D. G.; Lian, T.; Hill, C. L. *J. Am. Chem. Soc.* **2009,** 131, 7522-7523. (b) Huang, Z.; Geletii, Y. V.; Musaev, D. G.; Hill, C. L.; Lian, T. *Ind. Eng. Chem. Res.* **2012,** 51, 11850-11859. (c) Kaledin, A. L.; Huang, Z.; Geletii, Y. V.; Lian, T.; Hill, C. L.; Musaev, D. G. *J. Phys. Chem. A* **2010,** 114, 73-80.

[7] (a) Natali, M.; Orlandi, M.; Berardi, S.; Campagna, S.; Bonchio, M.; Sartorel, A.; Scandola, F. *Inorg. Chem.* **2012,** 51, 7324-7331. (b) La Ganga, G.; Puntoriero, F.; Campagna, S.; Bazzan, I.; Berardi, S.; Bonchio, M.; Sartorel, A.; Natali, M.; Scandola, F. *Farad. Discuss.* **2012,** 155, 177-190.

[8] (a) Orlandi, M.; Argazzi, R.; Sartorel, A.; Carraro, M.; Scorrano, G.; Bonchio, M.; Scandola, F. *Chem. Commun.* **2010,** 46, 3152-3154. (b) Pizzolato, E.; Natali, M.; Posocco, B.; Montellano Lopez, A.; Bazzan, I.; Di Valentin, M.; Galloni, P.; Conte, V.; Bonchio, M.; Scandola, F.; Sartorel, A. *Chem. Commun.* **2013,** 49, 9941-9943.

[9] (a) Song, F.; Ding, Y.; Ma, B.; Wang, C.; Wang, Q.; Du, X.; Fu, S.; Song, J. *Energy Environ. Sci.* **2013,** 6, 1170-1184. (b) Han, X.-B.; Zhang, Z.-M.; Zhang, T.; Li, Y.-G.; Lin, W.; You, W.; Su, Z.-M.; Wang, E.-B. *J. Am. Chem. Soc.* **2014,** 136, 5359-5366.

[10] (a) Car, P.-E.; Guttentag, M.; Baldridge, K. K.; Alberto, R.; Patzke, G. R. *Green Chem.* **2012,** 14, 1680-1688. (b) Kaveevivitchai, N.; Chitta, R.; Zong, R.; El Ojaimi, M.; Thummel, R. P. *J. Am. Chem. Soc.* **2012,** 134, 10721-10724.

[11] Lv, H.; Song, J.; Geletii, Y. V.; Vickers, J. W.; Sumliner, J. M.; Musaev, D. G.; Kögerler, P.; Zhuk, P. F.; Bacsa, J.; Zhu, G.; Hill, C. L. *J. Am. Chem. Soc.* **2014,** 136, 9268-9271.

[12] Parent, A. R.; Crabtree, R. H.; Brudvig, G. W. *Chem. Soc. Rev.* **2013,** 42, 2247-2252.

[13] (a) Henbest, K.; Douglas, P.; Garley, M. S.; Mills, A. *J. Photochem. Photobiol.* **1994,** 80, 299-305. (b) White, H. S.; Becker, W. G.; Bard, A. J. *J. Phys. Chem.* **1984,** 88, 1840-1846.

[14] Rybak, W.; Haim, A.; Netzel, T. L.; Sutin, N. *J. Phys. Chem.* **1981,** 85, 2856-2860.

[15] (a) Ghosh, P. K.; Brunschwig, B. S.; Chou, M.; Creutz, C.; Sutin, N. . *J. Am. Chem. Soc.* **1984,** *106*, 4772-4783. (b) Limburg, B.; Bouwman, E.; Bonnet, S. *ACS Catal.* **2016,** 6, 5273-5284.

[16] (a) Romain, S.; Bozoglian, F.; Sala, X.; Llobet, A. *J. Am. Chem. Soc.* **2009,** 131, 2768-2769. (b) Bozoglian, F.; Romain, S.; Ertem, M. Z.; Todorova, T. K.; Sens, C.; Mola, J.; Rodríguez, M.; Romero, I.; Benet-Buchholz, J.; Fontrodona, X.; Cramer, C. J.; Gagliardi, L.; Llobet, A. *J. Am. Chem. Soc.* **2009,** 131, 15176-15187.